INFRARED THERMOGRAPHY PROCEDURE FOR BOUNDARY LAYER TRANSITION DETECTION

Mirko Zaccara, Leonardo Helicopters, Samarate (VA), Italy
Gabriele Giuseppe Campanardi, Leonardo Helicopters, Samarate (VA), Italy
Piergiorgio Scavella, Università degli Studi di Napoli "Federico II", Napoli (NA), Italy
Carlo Salvatore Greco, Università degli Studi di Napoli "Federico II", Napoli (NA), Italy
Gennaro Cardone, Università degli Studi di Napoli "Federico II", Napoli (NA), Italy

Abstract

Laminar to turbulent transition detection and control is a crucial aspect when designing aerodynamic shapes and assess their qualities. Many unpredictable factors present in general fluid dynamics phenomena determine the uncertainty of its estimation. A large spread of experimental techniques has been developed, and ever finer methods are used to be more confident with transition prediction. Infrared Thermography is one of the more suitable techniques when dealing with requirements like non-intrusive testing. It provides spatially resolved measurement and also real-time analyses. In this work, many experiments are performed with Infrared Thermography to detect transition on a generic wing at several angles of attack by using a particular condition on the inflection point of the temperature profile in the chordwise direction.

1. NOTATION

Symbols

c	Heat capacity, $\mathrm{J/kgK}$
c_f	Wall skin friction coefficient
d_p	Thermal penetration depth, m
h	Convective heat flux coefficient, $\mathrm{W/m^2}K$
k	Thermal conductivity, $\mathrm{W/mK}$
q_c	Convective heat flux, $\mathrm{W/m^2}$
q_r	Radiative heat flux, $\mathrm{W/m^2}$
q_w	Wall heat flux, $\mathrm{W/m^2}$
s	Model thickness, m
t	Time, s
T_{aw}	Adiabatic wall temperature, K
T_w	Wall temperature, K
T_{wi}	Initial wall temperature, K
α	Thermal diffusivity, $\mathrm{m^2}/s$
μ	Dynamic viscosity, $\mathrm{Pa \cdot s}$
ξ	Streamline tangent unit vector
ρ	Density, kg/m^3
τ	Wall shear stress
φ	Normalized temperature rise, K

Acronyms:

BL	Boundary Layer
CFD	Computational Fluid Dynamics
IRT	Infrared Thermography

2. INTRODUCTION

It is well known that the laminar–turbulent transition of the Boundary Layer (BL) is one of the key factors considered while optimizing the aerodynamic performance of vehicles or lifting bodies. While laminar flow offers advantages in terms of reduced drag and improved efficiency (Ref. [1]), turbulent flow can be beneficial in certain scenarios, such as in delaying or flow separation, enhancing the aerodynamic characteristics of the vehicle, particularly at high angles of attack or while maneuvering.

As far as wind tunnel testing is concerned, the estimation of the transition position could help in the correction procedure for the wind tunnel scaling effect but also the continuous improvement and tuning of the Computational Fluid Dynamics (CFD) methods and correlation with the experimental results, together with the assessment of boundary layer control techniques. However, the experimental detection of the BL transition and its prediction through computational tools is highly complex due to unpredictable external factors that trigger instabilities like acoustic noise, free stream turbulence, non-uniformity of actual surface, etc.

Several experimental techniques have been developed over the years involving different principles. Mechanical methods like oil flow visualization involves the use of oil pigment present on a solid surface immersed in a flow field to qualitatively track flow patterns and typologies (Ref. [2] [3]). Although these technologies are widely used as a qualitative method for flow visualization and for determining macroscopic quantity like skin friction, pressure, and temperature, it requires skill and experience to interpret the results (Ref. [4] [5] [6]).

Surface hot film anemometry is another extensively used electrical technique for turbulence analysis (Ref. [7]), which consists of an insulating and isolating material with very thin electrically conducting traces on its surface. By maintaining constant the temperature of these traces through the regulation of electrical current, the technique enables the determination of heat transfer from film surface into the boundary layer based on the variation of the conductors' resistance. Despite this sensors are generally characterized by higher accuracy measurement, their applicability and spatial resolution are limited by the sensor's dimensions.

As optical methodologies, InfraRed Thermography (IRT) technique stands out for its wide use and applications as a standard tool for the detection of static transition positions since it is a non-contact and non-intrusive technique which makes it particularly convenient for wind tunnel testing (i.e. it does not disturb the flow). In addition, IRT cameras are fully two-dimensional and they are characterized by high spatial resolution (up to 1 M pixels), high sensitivity (down to 20 mK) and low response time (down to 20 µs) which allow for convective heat transfer measurements with both steady and transient techniques. Furthermore, the IRT technique may not necessitate model painting and could potentially require no specialized surface preparation, offering also the potential for consecutive measurement of multiple test points in a single tunnel run. Although they differ in many aspects depending on the specific application, IRT methods fundamentally exploit the idea that turbulent and laminar boundary layers have different heat transfer behavior and that there is a close relationship between skin friction and heat flux at the wall (Ref. [8]). In fact, turbulence increases wall friction and convective heat transfer coefficient due to enhanced mixing momentum and energy exchange associated with turbulent flow structures. Therefore, adiabatic wall temperature rises albeit less significantly. As such, understanding convective heat transfer coefficient h and adiabatic wall temperature T_{aw} distribution offers insights into boundary layer states, useful for aerodynamic analyses. Generally, due to the increase of about four times of the surface heat transfer with a turbulent boundary layer, a qualitative evaluation of the surface temperature distribution allows to differentiate between the laminar and turbulent regions of the BL. When operating in subsonic flow with low kinetic heating, an external heat source is necessary to conduct quantitative IR measurements with different techniques like pre-heating the model (Ref. [9] [10]) or using continuous-pulsing source such as internal electrical devices [8], heating sheets (Ref. [11]), and heat lamp (Ref. [12]). The heat lamp technique with a portable infrared camera employed in the present work represents a tool with a high potential in industrial applications to detect transition on static models due to its simplicity and portability.

The description of the methodology adopted in the present work is reported in Section 3 detailing both the qualitative and the quantitative criterion for the laminar to turbulent transition detection. The experimental setup of wind tunnel and infrared thermography measurement is described in Section 4 together with the procedure employed for the heat transfer evaluation. Finally, the results are reported in Section 5 in terms of two dimensional temperature maps, temperature profile (both spatial and temporal) and their corresponding heat transfer coefficient evolutions. Then, some conclusions are drawn in Section 6.

3. METHODOLOGY

In the current work, a wing scaled model representative of a helicopter horizontal tailplane is worth as thin film sensor (Ref. [13]). In this regards, the output of the IRT camera pointing to the model can be considered as originated from a large array of small and thin resistance thermometers arranged in a two-dimensional way. A sketch of the thermal model is reported in Figure 1.

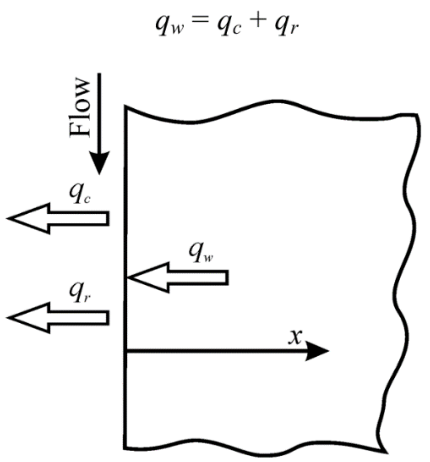

Figure 1: Sketch of the thin film sensor from Ref. *[13]*. In the current work, the radiative heat flux has an inverse direction since the model is heated. The x direction is inside the airfoil thickness.

The analytical model can be derived starting from one-dimensional solution for a semi-infinite wall having an initial constant temperature, which is then subjected to a heat flux on its surface given by the sum of convective and radiating contributions. In order to evaluate the effect of the finiteness of the real model and to ensure that the front surface is not influenced by the thermal phenomena of the other side of the model, in Ref. [13] an analysis is conducted on the time limit for which the heat wave from the back surface has not reached yet the front one in which we are interested in. It is evaluated as $s^2/3\alpha$, where s and α are the model thickness and the material thermal diffusivity respectively. Alternatively, if the penetration depth $\sqrt{\alpha t}$ is less than $s/\sqrt{3}$, a slab employed as a thin film heat flux sensor can closely mimic the characteristics of the semi-infinite wall model, with an error of 1% on temperature slab distribution.

From a quantitative analysis of the transition detection, it is required to evaluate the convective heat flux q_c acting on the surface under analysis. As such, by supposing that the slab is isothermal at the initial time of measurement at the temperature T_{wi}, it is possible to evaluate the wall heat flux q_w as a function of time using the model introduced by Cook and Felderman in Ref. [14] applied on the front surface temperature evolution $T_w(t)$ acquired with the infrared camera as:

$$q_w = \sqrt{\frac{\rho c k}{\pi}}\left(\frac{\varphi(t)}{\sqrt{t}} + \int_0^t \frac{\varphi(t)-\varphi(\tau)}{(t-\tau)^{\frac{3}{2}}}\,d\tau\right) \quad (1)$$

where ρ, c, k are the material density, heat capacity, and thermal conductivity respectively and $\varphi(t) = T_w(t-t_i) - T_w(t_i)$ is the normalized temperature variation.

As already mentioned, the wall heat flux is composed by two contributions: the convective q_c and the radiative q_r heat flux. In order to estimate the convective heat transfer, the radiative one should be calculated and there are two possibilities for carrying out the experiment:

1. $q_r = 0$: the radiative heat source during infrared camera acquisition is idle. In that case, model preheating is needed to generate the difference between surface temperature and free stream. The acquisition - or the analysis - must start when the wind tunnel acceleration phase is terminated and a steady state flow field is established;
2. $q_r \neq 0$: the radiative heat source is active during the acquisition. No model preheating is needed because the temperature differences are established since heating is used (i.e. through a halogen lamp or internal heating element). In order to extract the convective heat flux, the radiative heat flux must be estimated: a twin pair of experiments must be performed, one without the wind tunnel flow, since the Eq. (1) is used firstly to estimate q_r, the second with the wind tunnel on to estimate the whole heat flux at the wall and thus the convective one q_c since $q_w = q_c + q_r$ as reported also in Figure *1*.

In the present work, the second case is verified, so a temperature transient behavior must be settled in order to use the Eq. (1). For the sake, the experimental procedure is described in details in Section 4.

From a qualitative analysis of the transition detection, as reported by Arthur D. Woodworth et al. in Ref. [15] on the Reynolds analogy for a more general case, it exists an inverse proportionality between the wall shear stress τ and the temperature gradient ∇T as follows.

$$\tau \cdot \nabla T = \mu f_q \tag{2}$$

Thus, by projecting the Eq. (2) into the streamline reference frame, the normal component in that frame could be neglected, while the function f_q can be considered constant with the heat flux. Being ξ the streamline tangent unit vector, the Eq. (2) can be rewritten as:

$$\tau_\xi \cdot \frac{\partial T}{\partial \xi} = \left(\mu f_q\right)_\xi \tag{3}$$

By differentiating Eq. (3) it is possible to obtain a relationship between wall shear stress derivative and temperature second derivative as reported in Eq. (4) where C is a constant.

$$\frac{\partial T_\xi}{\partial \xi} = \frac{C}{\left(\frac{\partial T}{\partial \xi}\right)^2} \frac{\partial^2 T}{\partial \xi^2} \tag{4}$$

Therefore, this relationship between wall shear stress, or skin friction coefficient, and temperature leads to a qualitative criteria to detect transition onset. When the skin friction coefficient has reached the local maxima or local minima, the temperature profile has an inflection point.

$$\text{min / max } c_f \rightarrow \frac{\partial^2 T}{\partial \xi^2} = 0 \tag{5}$$

4. EXPERIMENTAL SETUP

The experiments were performed in a closed loop open jet wind tunnel (see Figure 2) with a test section 0.6 x 0.9 x 1 meters with a low level of turbulence ($Tu = 0.1\%$) evaluated with hot-wire anemometry. The test model is a rectangular wing, with a general airfoil as section, as reported in Figure 2.

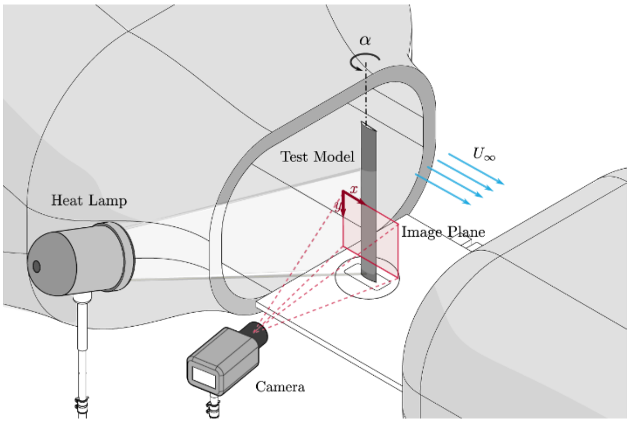

Figure 2: Sketch of the experimental setup. The wing basis is encapsulated in a PLA printed support which sets the right angle between the asymptotic wind tunnel flow and the wing.

All the tests are performed at a wind speed of $30\ m/s$ with a reference Reynolds number of about 140.000. To set the desired angle of attack, the test model is vertically installed onto a turning table. The model, made of ceramic-based 3D printed material with low thermal conductivity, is heated almost uniformly by a halogen lamp with a maximum power of 1000 W, positioned at 20 chords from the test section center and aligned perpendicularly with respect to the flow direction. The employed IR camera is the FLIR T650sc, with a resolution of 640 x 480 pixels, a sensitivity range of 7.5-13, and an acquisition frequency of 30 Hz. The estimated spatial resolution was about 2 pixels/mm.

4.1. Experimental Procedure

According to the adopted methodology, a semi-infinite wall model is considered and its application should be checked. As such, in Table 1 the estimated thermal properties of the material are reported since it is a property material and official data can not be shared from the supplier. For the same reason, as reference airfoil section a NACA 63-412 has been considered.

Table 1: Estimated material properties.

ρ	c	k	α
Kg/m^3	J/kgK	W/mK	m^2/s
1610	1500	0.31	$1.28 \cdot 10^{-7}$

For all test cases analyzed the heating time is set to 13 seconds and the penetration depth is calculated as follows.

$$d_p = \sqrt{t_m \alpha} = 0.13cm = 0.015chord \tag{6}$$

In Figure 3 is reported the time for which we admit an error of 1% on temperature distribution using as slab thickness the airfoil thickness distribution. It is reported also the measurement time from the heating start as a dashed line. Within the 86% of the chord, by measuring for 13 seconds, a small error is obtained with the semi-infinite slab model, thus the measurements can be relied on. On the other hand, at the Trailing Edge (T.E.) of the airfoil, a larger error is admitted in considering the semi-infinite model instead of considering the presence of the finite thickness since the heat wave of the back surface is reaching the front model surface.

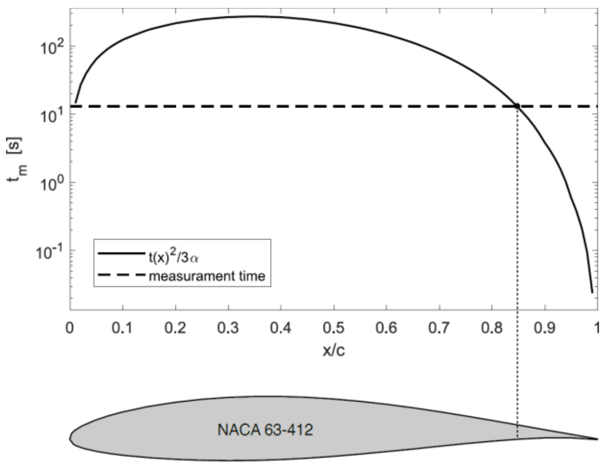

Figure 3: Time for which an error of 1% on temperature distribution is assumed using as slab thickness the airfoil thickness distribution.

As already mentioned in section 3, a twin pair of experiments are performed for each angle of attack of the model for a duration of 15 seconds. In particular:

- A first experiment in which the wind tunnel is off and the model is isotherm at ambient temperature. Then, the halogen lamp is turned on after 2 seconds from the acquisition start. As such, from Eq. (1), the radiative heat flux q_r is estimated since it corresponds to the whole wall heat flux ($q_c = 0$);
- A second experiment in which the wind tunnel is on and the model is in thermal equilibrium with the flow. The halogen lamp is again turned on after 2 seconds from the acquisition start and the temperature transient is established. Via Eq. (1), is now possible to estimate the convective heat flux q_c since the radiative term q_r is already known.

As a matter, the convective heat flux q_c is estimated for each point of the surface in time, thus the convective heat transfer coefficient can be evaluated as follows for a quantitative analysis:

$$(7) \qquad h(x,y,t) = \frac{q_c(x,y,t)}{T_w(x,y,t) - T_w(x,y,t_i)} \ .$$

In the present work, several angles of attack are tested at the same Reynolds number but only few of them are reported hereinafter for brevity. There have been performed two sets of experiments: one with a clean surface for the sake of estimating the free transition onset, and the other with transition dots of 0.25mm of diameter and a spacing of two diameters attached at 5% of the chord to estimate their effectiveness in forcing the transition bypass..

5. RESULTS

A typical acquired infrared image is shown in Figure 4Figure 4. For this case the transition has no tripping and the angle of attack is set to $\alpha = 0°$. The temperature profile over time of the extracted slice is reported in Figure 5: after 2 seconds from the acquisition start, the heat lamp is turned on and the temperature rises.

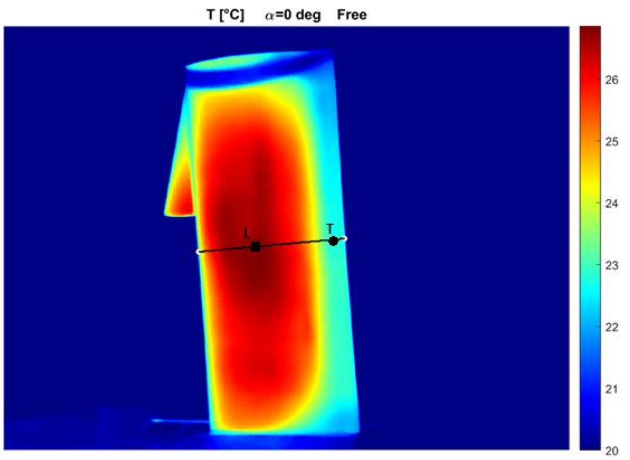

Figure 4: Temperature map for $\alpha = 0°$, free transition case at 10 second after lamp heating. The black line is a slice on which temperature is extracted. The square indicates a laminar point and the circle a turbulent one. The wind is flown from left to right.

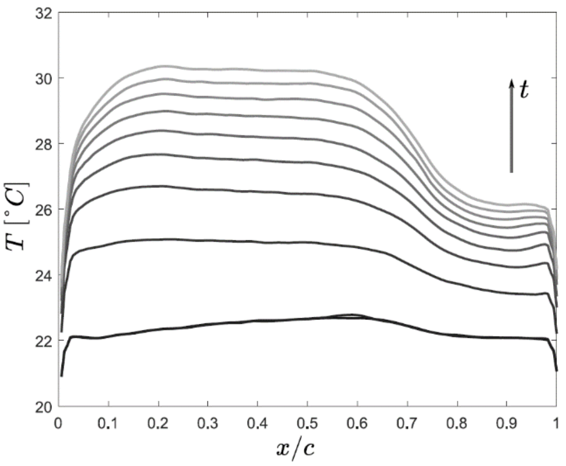

Figure 5: Temperature profile over time for $\alpha = 0°$ on the slice depicted in Figure 4, free transition case. The time increases as the temperature profile increases its mean value, and the curve color becomes brighter.

In particular, in Figure 6, the normalized temperature rise comparison between the laminar and turbulent point is reported. It is possible to note how the convection tends to cool down the model surface, with respect to the case without flow, where only natural convection and radiative heat flux are present (further internal conduction is present in every case). Furthermore, it is clear that the turbulent regime, which has a higher heat transfer coefficient, has also better cooling behavior due to the lower temperature derivative of time temperature evolution.

For the sake of brevity, only few angle of attack are analyzed ($\alpha = -6°, -2°, 0°, 4°, 8°, 12°$) and the results are reported referring to a single time instant of 10 seconds after the heat lamp is turned on. On each temperature profile reported hereinafter, the transition onset point is evaluated with the condition of minimum temperature spatial derivative from Eq. (5). The noise present in the temperature measurement affects the transition detection with the previous criteria. To avoid this error a moving average in time is applied to the prediction of transition position and the initial wall temperature is subtracted in each point. Moreover, to enhance the automation level of the algorithms, a mask is automatically generated for each temperature map to remove the background to avoid catching an inflection point on the temperature in the space around the wing body.

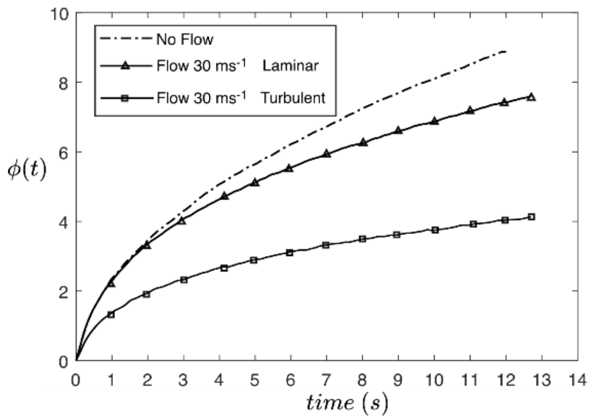

Figure 6: Normalized temperature variation over time for $\alpha = 6°$ in the laminar point reported in Figure 4, for in the free transition case compared with the turbulent point.

The free transition cases results are reported in Figure 7. For each angle of attack, the temperature map is cut to the relevant part of the IRT field of view; the temperature profile reported below in the left is referring to the slice depicted as vertical black line in the temperature map and its corresponding heat transfer coefficient profile is in the bottom-right location. The transition point is depicted as a black cross and red dot in the temperature map and profile respectively. It is worth noting that the temperature inflection point detected with the previous criterion is projected on the convective heat transfer coefficient curve as double-checking, useful to ensure that the transition point qualitatively detected has also a physical meaning (i.e. could be found in the h inflection point position).

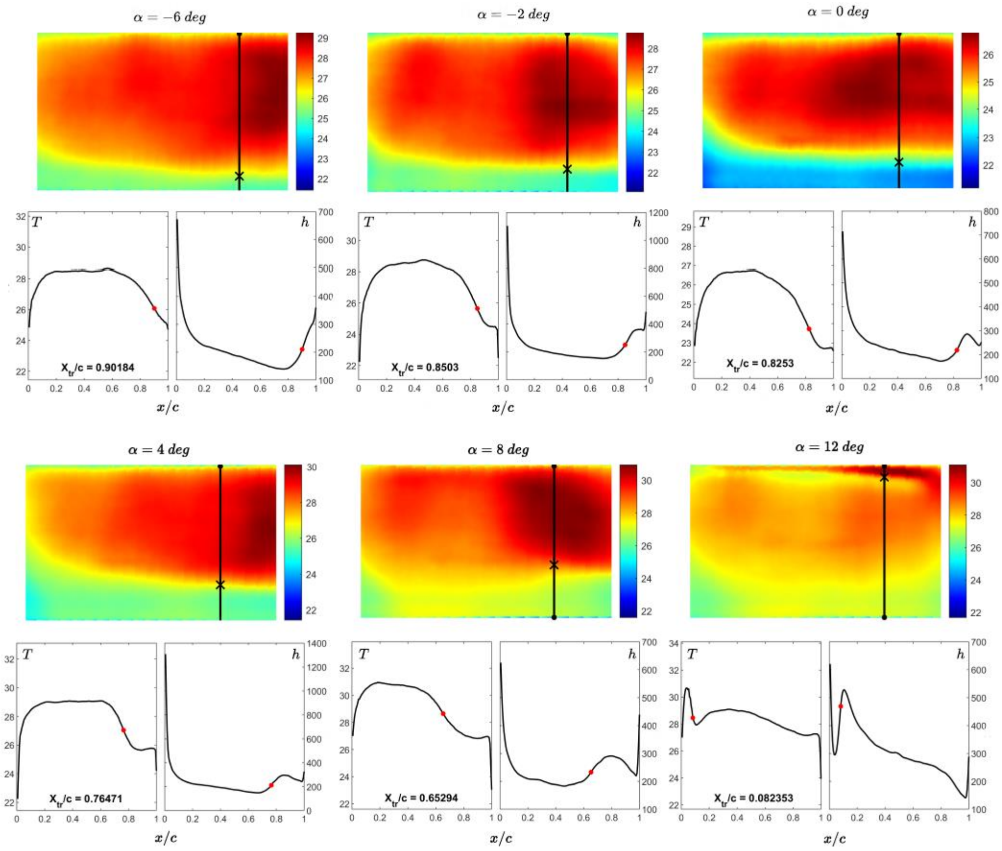

Figure 7: Temperature maps and data reduction for $\alpha = -6^{\circ}, -2^{\circ}, 0^{\circ}, 4^{\circ}, 8^{\circ}, 12^{\circ}$, free transition case.

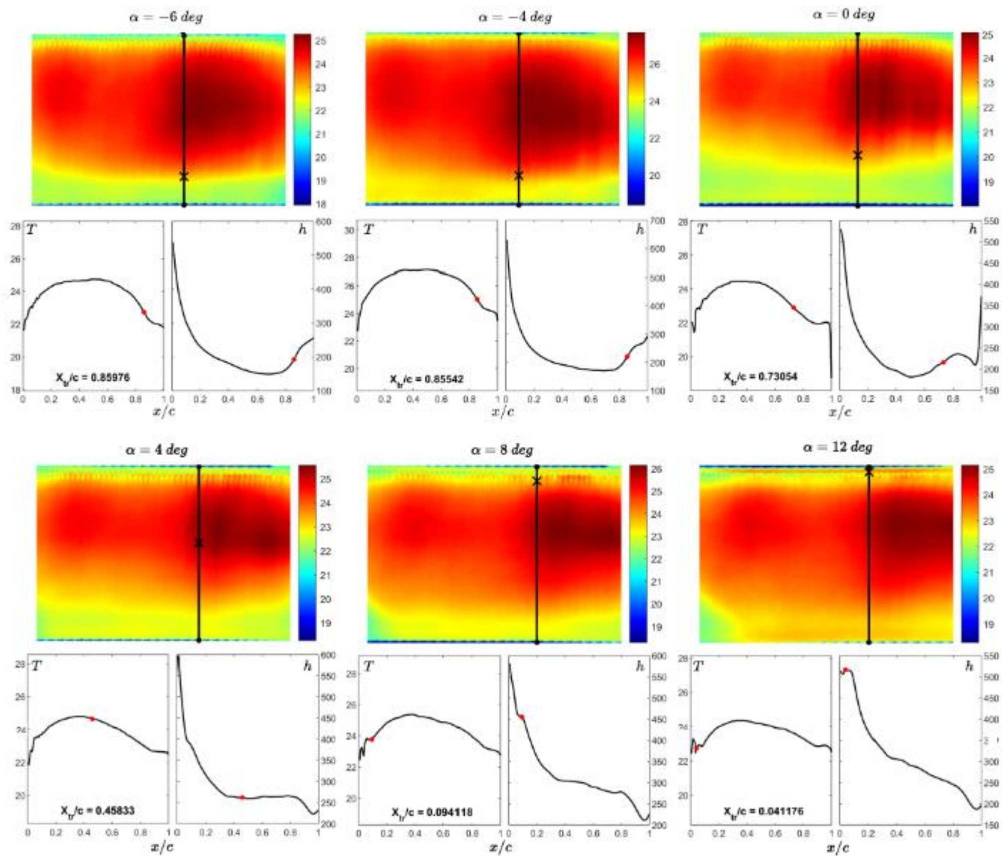

Figure 8: Temperature maps and data reduction for $\alpha = -6^{\circ}, -2^{\circ}, 0^{\circ}, 4^{\circ}, 8^{\circ}, 12^{\circ}$, forced transition case.

For negative angle of attack, the transition is detected on the rear part of the wing, and its position shifts forward as α increases. In the convective heat transfer coefficient curve appears an inflection point even though the effect of low thickness of the trailing edge hides the turbulent branch, especially in the case of $\alpha = -8°$ and $\alpha = -6°$.

At $\alpha = -2°$, the inflection point becomes evident from the temperature profile while it appears a change in h trends at the end of the airfoil. This transition of h from laminar to turbulent state is more evident for $\alpha = 0°$, showing that as the angle increases the transitional behavior shifts forward.

Increasing the angle of attack to $\alpha = 4°$, the temperature profile shows a laminar evolution up to $x/c \approx 0.65$ where the transition onset appears as an increasing derivative. Then, the flex point is detected at $x/c \approx 0.76$ assumed as the transition point, confirmed with the presence of the flex point on the convective heat transfer coefficient too. In the latter, the maxima at $x/c \approx 0.80$ indicates the beginning of the turbulence branch.

Almost the same evolution is found at $\alpha = 8°$ although the transition occurs earlier and it is more evident.

From $\alpha = 12°$ a laminar separation bubble is clearly present if Figure 7. The presence of the latter can be justified with the typical shape of h with a laminar descent, a flex point indicating the separation (not visible due to the low spatial resolution), the presence of minima where the transition process begins and the rise to the maximum in correspondence to the reattachment point. The latter can be explained by the shear stress and convective heat transfer analogy since a strong wall shear stress at the reattachment corresponds a high heat transfer coefficient.

The forced transition case temperature map, temperature profile, and convective heat transfer coefficient profile are reported in Figure 8. The dots wakes are evident both in the temperature map and in the temperature profile as a non-regularity of temperature rises itself. A classical transition shape on h is present up to $\alpha = 0°$. For higher angles of attack (e.g. $\alpha = 4°$) there is no net transition but could be individuated a region where the laminar to turbulence transition process is spread on more length in the streamwise direction and the beginning of the transition process can be found anticipated at $x/c \approx 0.4$ with respect to the free transition case. As the angle of attack α increases, it seems that the tripping dots cause the direct bypass of the transition process while h behaves descending on the whole length of the airfoil like in the turbulent branch, even though it is not regular. In fact, at $\alpha = 8°$, it seems that the flow evolves with the turbulent branch earlier with respect to the free case. Lastly, a $\alpha = 12°$, the separation bubble is present also in the forced case, and the main effect of the tripping dots is to delay the laminar bubble formation which results in an earlier reattachment point with respect to the free case.

6. CONCLUDING REMARKS

A series of experiments are performed through IRT to determine the transition from laminar to turbulent on a wing model representative of a horizontal tailplane of a helicopter starting from infrared thermography images. The criterion used to detect the transition point was defined through qualitative investigations using the temperature data only with the detection of the inflection point of its profile. Through the experimental double test procedure, it was also possible to carry out a quantitative analysis by estimating the convective heat transfer coefficient. These latest investigations revealed to be useful for validating the qualitative criterion on temperature. Indeed, for cases of natural transition, the transition point estimated through the temperature inflection criterion appears to be consistent with the distribution of the convective heat transfer coefficient h. This is not always verified, especially for cases of forced transition, where the behaviors of the heat transfer are no longer similar to the classical ones, and the wakes of tripping sots strongly influence the evolution of the boundary layer.

Generally, it is clear that for the natural transition case, the position of the onset transition advances, moving to the airfoil leading edge when the angle of attack increases. As it can be noted at $\alpha = 0°$ angle of attack, the separation region at the wing root is clearly visible together with the transition region which arises around the 75% of the chord where the temperature second derivative reaches a null value and it is constant along the span up to the tip region. As On the other hand, the presence of the transition causes a trigger of the boundary layer transition which turns out in early transition around 65% of the chord. Even though the maximum of temperature profile seems to occur at the same x/c position for both free and forced transition, the temperature profile of the latter has different spatial evolution in terms of constant gradient from the maximum to the minimum value. Increasing the angle of attack to $\alpha = 12°$, the presence of a laminar bubble can be identified by the steep rate of the temperature rise, which is caused by a convective heat transfer dropped down by the recirculation inside the bubble. The forced transition strips influences only locally the boundary layer causing a premature turbulent reattachment of laminar bubble in correspondence of the local minima of the temperature profile at around 12% of the chord.

However, the results of the present work highlight the versatility of the technique and its measurement procedure and also the possible use for more complex industrial applications, also due to the portability of the instruments and the non-intrusiveness of the experimental technique. As far as future works regard, there is still room to improve the quality of the post-processed data based on the recent literature on this topic especially when dealing with different heat transfer problems to evaluate the convective heat transfer coefficient. The latter surely represents an added value allowing a better and valuable interpretation of the results which could be compared with already available data from CFD and flight data from the installed solution on a complete aircraft.

Author contact:

Mirko Zaccara, mirko.zaccara@leonardo.com

Gabriele Giuseppe Campanardi, gabrielegiuseppe.campanardi@leonardo.com

Piergiorgio Scavella, piergiorgio.scavella@unina.it

Carlo Salvatore Greco, carlosalvatore.greco@unina.it

Gennaro Cardone, gennaro.cardone@unina.it

7. REFERENCES

1. M. N. Lynde, R. L. Campbell, M. B. Rivers, S. A. Viken, D. T. Chan, S. L. Watkins and S. L. Goodliff, "Preliminary results from an experimental assessment of a natural laminar flow design method," in *AIAA Scitech Forum*, 2019.

2. J. Dagenhart, J. Stack, W. Saric and M. Moussex, "Crossflow-vortex instability and transition on a 45 deg swept wing," in *20th Fluid Dynamics Plasma Dynamics and Lasers Conference*, 1989.

3. T. Liu, "Global skin friction measurements and interpretation," *Progress in Aerospace Sciences,* vol. 111, 2019.

4. F. Lu, "Surface oil flow visualization: Still useful after all these years," *The European Physical Journal Special Topics,* vol. 182, no. 1, pp. 51-63, 2010.

5. L. Langston and M. Boyle, "A new surface-streamline flow visualization technique," *Journal of Fluid Mechanics,* vol. 125, pp. 53-57, 1982.

6. M. J. Délery, "Robert legendre and henri werlé: toward the elucidation of three-dimensional separation," *Annual review of fluid mechanics,* vol. 33, no. 1, pp. 129-154, 2001.

7. D. Rudmin, A. Benaissa and D. Poirel, "Detection of laminar flow separation and transition on a naca-0012 airfoil using surface hot-films," *Journal of fluids engineering,* vol. 135, no. 10, pp. 101-104, 2013.

8. L. de Luca, G. M. Carlomagno and G. Buresti, "Boundary layer diagnostics by means of an infrared scanning radiometer," *Experiments in fluids,* vol. 9, no. 3, pp. 1187-1218, 1990.

9. Y. Yokokawa, "Transition measurement on metallic aircraft model in typical lowspeed wind tunnel," *JPN Soc. Aeronaut.,* vol. 48, 2005.

10. M. Grawunder, R. ReB and C. Breitsamter, "Thermoraphic transition detection for low-speed wind-tunnel experiments," *AIAA Journal,* vol. 54, no. 6, pp. 2012-2016, 2016.

11. B. K. Crawford, G. T. Duncan Jr, D. E. West and W. E. Saric, "Robust, automated processing of IR thermography for quantitative

boundary-layer transition measurements," *Experiments in Fluids,* vol. 56, 2015.

12. S. von Hoesslin, M. Stadlbauer, J. Gruendmayer and C. J. Kahler, "Temperature decline thermography for laminar turbulent transition detection in aerodynamics," *Experiments in fluids,* vol. 58, pp. 1-10, 2017.

13. T. Astarita and G. M. Carlomagno, Infrared Thermography for Thermo-Fluid-Dynamics, New York (USA): Berlin Heidelberg, 2013.

14. W. Cook and E. Felderman, "Reduction of data from thin film heat-transfer gages: a concise numerical technique," *AIAA Journal,* vol. 4, no. 3, pp. 561-562, 1966.

15. A. D. Woodworth, D. M. Salazar and T. Liu, "Heat transfer and skin friction: beyound the reynolds analogy," *International Journal of Heat and Mass Transfer,* vol. 206, 2023.